VOLUME 27, 2, 101–113
ASLE TRANSACTIONS
1984

An Optical Profilometer for Surface Characterization of Magnetic Media

JAMES C. WYANT and CHRIS L. KOLIOPOULOS
University of Arizona
Tucson, Arizona
and
BHARAT BHUSHAN (Member, ASLE) and ORRIN E. GEORGE
IBM Corporation
Tucson, Arizona

Conventional surface-characterization techniques either are not sophisticated enough to provide complete surface-topographical data or cannot be employed because of the relatively low hardness of magnetic media. An optical profilometer has been developed which provides a noncontact method of obtaining surface characteristics from a magnetic medium. The system consists of a standard Leitz reflection microscope, a Mirau interferometer controlled by a piezoelectric transducer, a linear array of photodiode detectors, and a microcomputer. The combination yields a system that measures the optical-height variations of surfaces to a high degree of precision. This height variation is processed by a computer to provide surface-topographical statistical parameters, which are useful to predict tribological and magnetic performances of the head-media interface. Sample data of magnetic media (tape, floppy disk, and rigid disk) are presented.

INTRODUCTION

The characterization of surface *microtopography* is important in the study of interfacial phenomena, such as friction and wear, thermal and electrical contact resistance, and other functional situations (*1*). The major thrust has been on defining and measuring surface-topography parameters that affect surface interaction (*2*) to (*5*).

Understanding the surface topography of magnetic head-medium interfaces is of great interest in conventional magnetic recording, where read/write functions are accomplished by the relative motion of a magnetic head and the medium (tape, rigid disk, or floppy disk). Continuous contact occurs between a head and a medium during start-stop and (in cases of tapes and rigid disks) a hydrodynamic film is generated when the moving member reaches a lift-off speed (which is lower than the speed used to read or write and rewind). Because linear-bit density and the resolution of recorded signals increase with decreased head/medium spacing, close proximity between the read/write head and the medium is essential. This generally results in occasional contact at the high asperities; therefore, the importance of surface characterization cannot be overemphasized.

A commonly used tool to measure surface topography is a stylus instrument that amplifies and records the vertical motions of a stylus as it is moved at a constant velocity across the surface to be measured. The diameter of the stylus is very small, typically 2 μm, to detect finer asperities. A load of about 25 mg is applied during tracing. This technique is quite adequate for hard materials. However, in case of polymers (magnetic media), the stylus digs into the surface and the results do not truly represent the surface's microtopography. Other less commonly used techniques to measure only "average" roughness are the pneumatic method (which measures the pneumatic resistance between a circular transducer and the surface), and the hydraulic method (which measures the time taken for a given volume of liquid to travel a given length of the surface measured).

For soft surfaces, noncontacting techniques such as optical and interference methods are preferable. High magnification SEM micrographs, both replica and reflection, were used by Williamson (*6*) to qualitatively reveal the surface's topography. A major US corporation has undertaken a study that uses stereoscopic image pairs generated by an SEM to define surface topography quantitatively. One method that has been commonly used for magnetic media (average surface roughness) is a glossmeter, which was initially developed by the paint and coating industry (ISO 2812 or ASTM D523). The glossmeter measures the specular reflectance (or gloss) of the surface (*7*). Gloss depends on both the refractive index of the surface and the surface texture. Therefore, gloss data are not a sole function of surface topography; at best it gives an average surface topography.

Both the differential interference contrast (DIC) and the Normarski polarization inteferometer techniques are useful for qualitative assessments of surface topography; however, quantitative results may be difficult to obtain (*8*), (*9*). For both systems, which are shearing interferometers, the specimen surface is referenced against itself. The difference

Presented at the 38th Annual Meeting in Houston, Texas, April 24–28, 1983

between the two images of the surface being examined is less than the resolution of the microscope objective being used, while for the Normarski interferometer the shear is large compared with the resolution of the objective, so that two superimposed displaced images are seen. While both techniques are easy to use, analysis of the test results is difficult, and surface details are observed only in the direction of shear.

The need for a better technique to measure quantitatively surface microtopography of soft magnetic media is obvious. This paper describes a noncontact measurement technique that uses the principle of Mirau interferometry, electronic-phase-measurement techniques, and computer analysis.

THEORY AND OPERATION OF THE OPTICAL PROFILOMETER

The optical profilometer described in this paper uses an interference microscope, modified to incorporate an optical phase-shifting device and a solid-state, linear array of 256 photodiode detectors, which provides the capability of accurate surface-height measurements. Using the linear detector array, surface profiles over a small region of a sample can be obtained, and surface-height measurements made available at each detector location. For random surface-roughness measurements, the surface-height data form a basis for statistical analysis; surface-height distributions, autocovariance functions, and spectral-density functions are all derived from the height data. Height, slopes, and curvatures of asperities can be calculated. The accurate height information can also be applied to peak-height measurements and radius of curvature measurements.

The heart of the optical profiling microscope is a Leitz Mirau interferometer (*10*). This interferometer is an attachment to a long-working-distance microscope's objective and operates in reflection. A schematic of the Mirau interferometer is shown in Fig. 1. Light from a tungsten light source is incident upon the Mirau objective which images the field stop onto the surface to be tested. The Mirau beamsplitter forms a second optical path which ends at the reference surface where an image of the field stop is also formed. By symmetry, if both the surface under test and the reference surface are at the image of the source, the optical-path length between the beamsplitter and the test surface will be equal to the optical path between the beamsplitter and the reference surface. Thus, a white light source can be used, because both paths are equal, and yield white light fringes. The test surface and the reference surface are imaged again onto the photodiode detector array, which measures the intensity distribution of the interference fringes across a linear section.

The Mirau interferometer (objective, reference, and beamsplitter plates) is mounted on a piezoelectric transducer (PZT). The PZT transducer provides a phase modulation by modulating the optical-phase difference between the test and the reference arms of the Mirau interferometer. While voltage is applied to the PZT transducer, the complete Mirau interferometer is moved closer to the surface under test, thus changing the relative phase difference between the reference arm and the test arm of the interferometer. This causes the interference fringes to shift in position. The PZT transducer is stepped three times, each step corresponding to 90° in phase difference between the test and the reference arms. After each step, the interference pattern from the interference of the wavefronts caused by the test surface and the reference surface is recorded by the photodiode detector array and stored in a microcomputer.

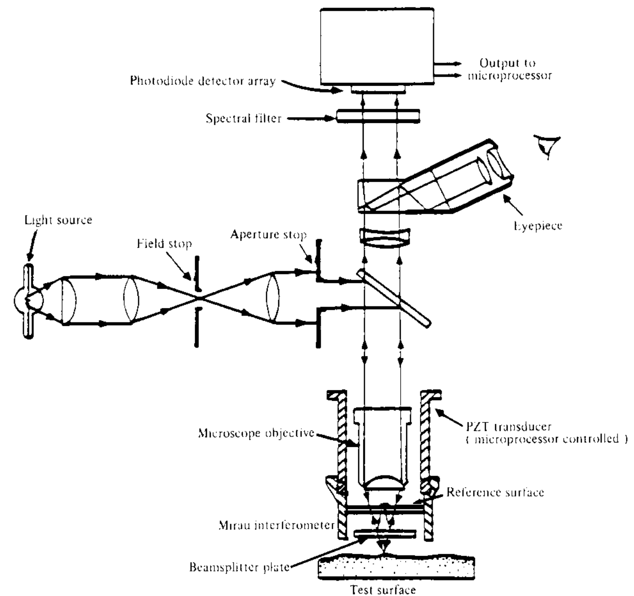

Fig. 1—Schematic of the optical profilometer

Figure 2 illustrates the instrumentation, which includes an 8-bit microcomputer that controls the detector readout. The detector output is digitized by a 12-bit A/D (analog/digital) converter, and the results are put into computer storage using a direct memory access (DMA) interface. The microcomputer then solves for the phase values (which are

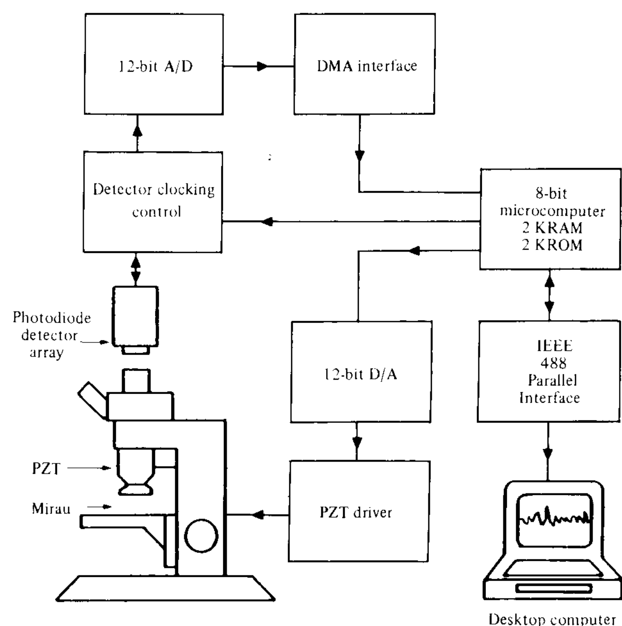

Fig. 2—Block diagram of the instrumentation and the processing system

proportional to the surface heights) after the three measurements by using the simple quadrature-phase algorithm described below. The microcomputer also controls the PZT transducer through a 12-bit D/A (digital/analog) converter. The calculated surface heights are then sent, via an IEEE 488 parallel interface, to a desktop computer.

The Mirau interferometer offers distinct advantages over other microscope-based, two-beam interferometers (See Table 1). For example, the Normaski and DIC interferometers are also commonly used with microscopes. While these interferometers are very easy to operate, and they are almost vibration-insensitive, they have the disadvantage that they both measure what is essentially the slope of the surface errors, rather than the surface errors themselves. Furthermore, because they measure surface slope errors in only one direction, sample orientation is very important.

Table 1—Advantages of Mirau Interferometer
Noncontact
Compact
Optically Simple
Common path through microscope objective
Three different reflectivity reference surfaces available without removing components
Yields surface errors rather than the slope of the surface errors

Phase Measurement

Several electronic-phase-measurement techniques can be used in an optical profilometer, *(11)* to *(13)*, to give much more accurate height measurement capability than can be obtained simply by looking at the interference fringes and measure how they depart from being straight and equally spaced. Two techniques that work rather well with solid-state detector arrays are the phase-stepping technique and the integrating-bucket technique. For both of these techniques, the phase of the reference beam is changed in a controlled manner by use of the PZT transducer shown in Fig. 1. Once the phase, $\phi(x,y)$, is determined across the interference field, the corresponding height distribution, $h(x,y)$, is determined by the equation

$$h(x,y) = \frac{\lambda\,\phi\,(x,y)}{4\pi} \qquad [1]$$

In the so-called three-step, phase-shifting technique for measuring phase, the detector array is first read out, then the phase of the reference beam is changed 90°, and the array is again read out. The phase of the reference beam is changed another 90° and the array is read out a third time. Equation [2] gives the irradiance that would be obtained at the three-phase steps separated by 90°. A 45° constant phase shift has been introduced to simplify the final equations for $\phi(x,y)$. This 45° constant phase shift has no effect upon the final result

$$\begin{aligned} A(x,y) &= I_1 + I_2 \cos[\phi(x,y) + \pi/4] \\ &= I_1 + I_2 \{\cos\phi(x,y) - \sin\phi(x,y)\}/\sqrt{2} \\ B(x,y) &= I_1 + I_2 \cos[\phi(x,y) + 3\pi/4] \\ &= I_1 + I_2 \{-\cos\phi(x,y) - \sin\phi(x,y)\}/\sqrt{2} \\ C(x,y) &= I_1 + I_2 \cos[\phi(x,y) + 5\pi/4] \\ &= I_1 + I_2 \{-\cos\phi(x,y) + \sin\phi(x,y)\}/\sqrt{2} \end{aligned} \qquad [2]$$

and

$$\phi(x,y) = \tan^{-1}\left\{\frac{C(x,y) - B(x,y)}{A(x,y) - B(x,y)}\right\} \qquad [3]$$

This phase measurement is performed at each detector point. Because of the subtraction and division, the effects of fixed pattern noise and gain variations across the detector are cancelled out, as long as the effects are not so large as to make the dynamic range of the detector too small to be of use. From Eq. [2], there are three unknowns, I_1, I_2, and $\phi(x,y)$, and three equations are needed to solve for $\phi(x,y)$ at each detector point.

It is not necessary that the phase step be 90°. If I_n is the intensity of the interference pattern obtained by stepping the phase an amount $n(2\pi/N)$, phase ϕ can be determined by using Eq. [4]. In this case, the resulting intensity I_n is multiplied by a cosine and sine and summed and divided to give the tan of the phase difference ϕ. This method is equivalent to synchronous-detection techniques in communication theory

$$\tan\phi = \sum_{n=1}^{N}\left\{I_n \sin[n(2\pi/N)]\right\} \Big/ \sum_{n=1}^{N}\left\{I_n \cos[n(2\pi/N)]\right\} \qquad [4]$$

A similar method for measuring the phase is the integrating-bucket technique *(14)*. In the integrating-bucket technique, the relative phase of the reference and test beams is varied at a constant rate rather than in discrete steps. For simplification of the electronics, the three-step, phase-shifting technique was used for all the measurements shown in the paper. However, in future instruments, the integrating-bucket technique will be used. The advantage of the integrating-bucket technique is that the reference surface is moved at a constant velocity rather than stepping it as the phase-shifting technique and hence the vibration introduced into the system is minimized.

If the signs of the numerator and denominator of the expression giving the $\tan\phi(x,y)$ are checked for either the phase-shifting or the integrating-bucket technique, the phase measurement can be performed modulo 2π. If more than one interference fringe is present in the interference pattern, a measurement performed modulo 2π can lead to ambiguities. However, this ambiguity can be resolved if the restriction is made that between any two adjacent detector points the phase must change by less than π; that is, the surface-height change between adjacent detector points *must be less than ¼ wavelength* ($\simeq$ 0.15 microns). Then, if the phase calculated for two adjacent points differs by more than π, 2π must be either added or subtracted to the second detector point to get the two adjacent phase values to differ by less than π. In this manner, ambiguities caused by having more than one interference fringe present can be resolved.

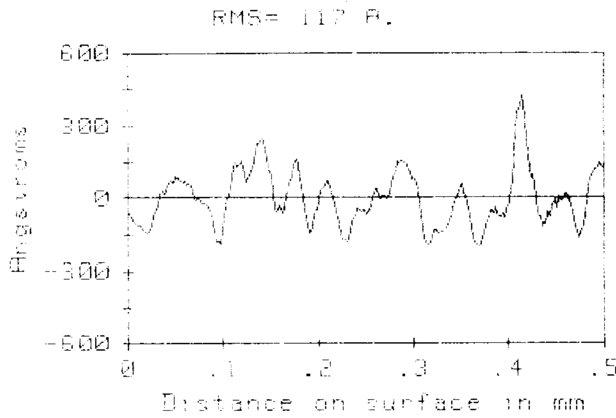

Fig. 3(a)—Surface profile for Tape A

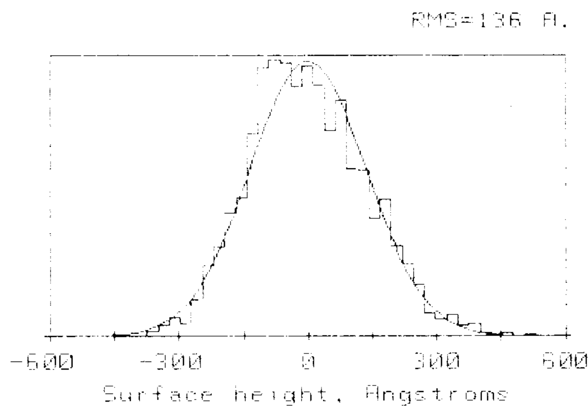

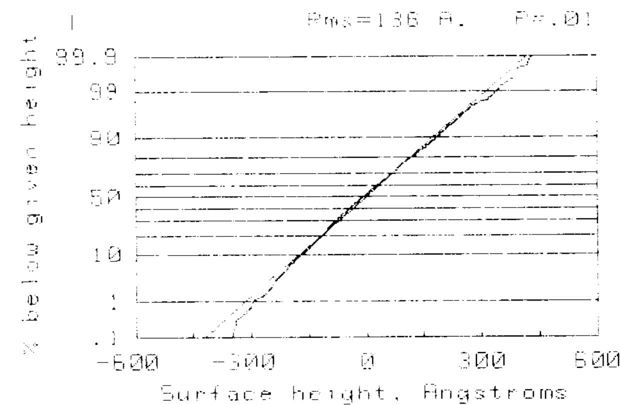

Fig. 3(b)—Histogram and distribution of surface heights for Tape A

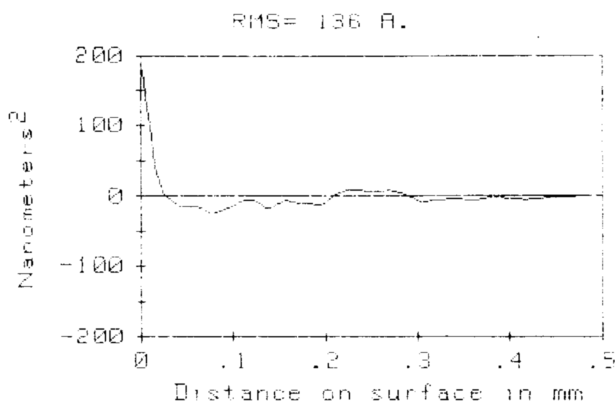

Fig. 3(c)—Autocovariance function for Tape A

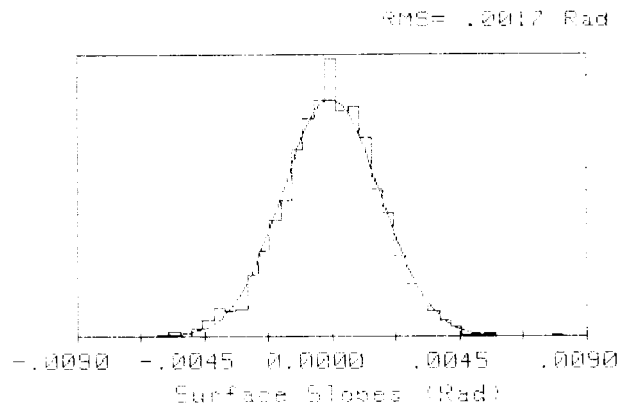

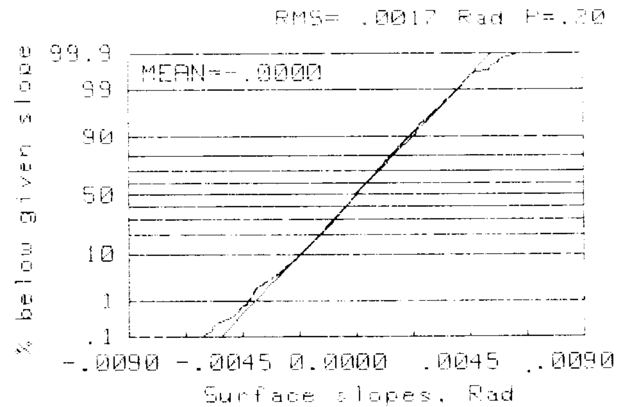

Fig. 3(d)—Histogram and distribution of surface slopes for Tape A

It should also be noted that there is never a question about the sign of the phase, and hence, whether the surface height is increasing or decreasing.

Data Analysis

Once the height distribution across the sample is measured, the data can be analyzed to determine many properties about the magnetic media being studied. Figure 3 consists of a series of plots we have found useful in studying the tribology of magnetic media, (*1*) to (*5*). The plots can be made for a single data set or for the average of many data sets. For all the plates shown in Fig. 3, except for the surface-profile plot, the results are for the average of 10 data sets, of 256 data points each. The profile plot is for a single data set of 256 data points. This section briefly describes the analysis used in obtaining each of the plots shown.

Surface Profile

The height distribution across the sample is fitted in a least-squares method to determine the average height, the tilt across the sample, and the curvature. The average height is always subtracted from the height distribution. Generally, the tilt is also subtracted because it is arbitrary and depends upon the adjustment (tip-tilt) of the reference surface in the interferometer. In the analysis of tape samples, the curvature is generally subtracted before the surface profile is plotted, because the curvature is the result of not holding the tape sample flat. The peak-valley distance (P-V) is determined by subtracting the lowest height measured from

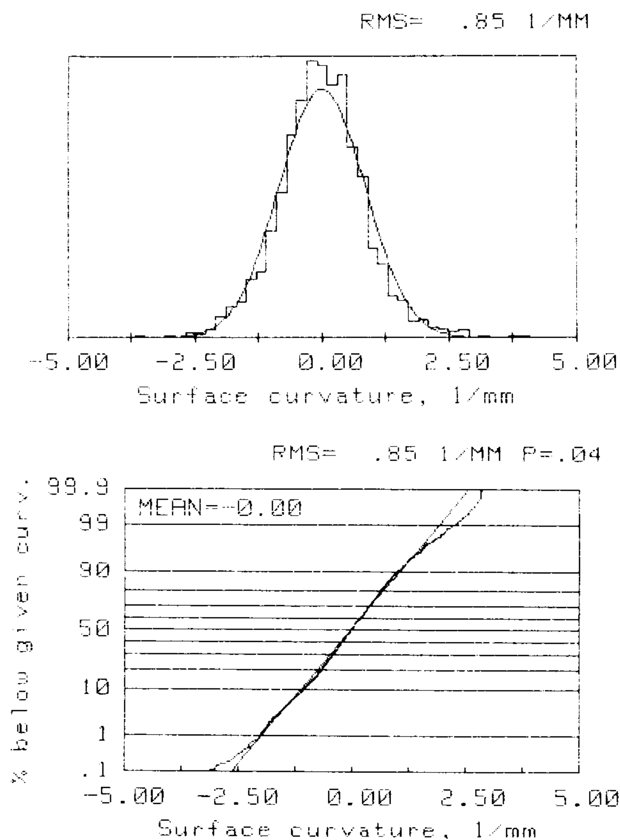

Fig. 3(e)—Histogram and distribution of surface curvature for Tape A

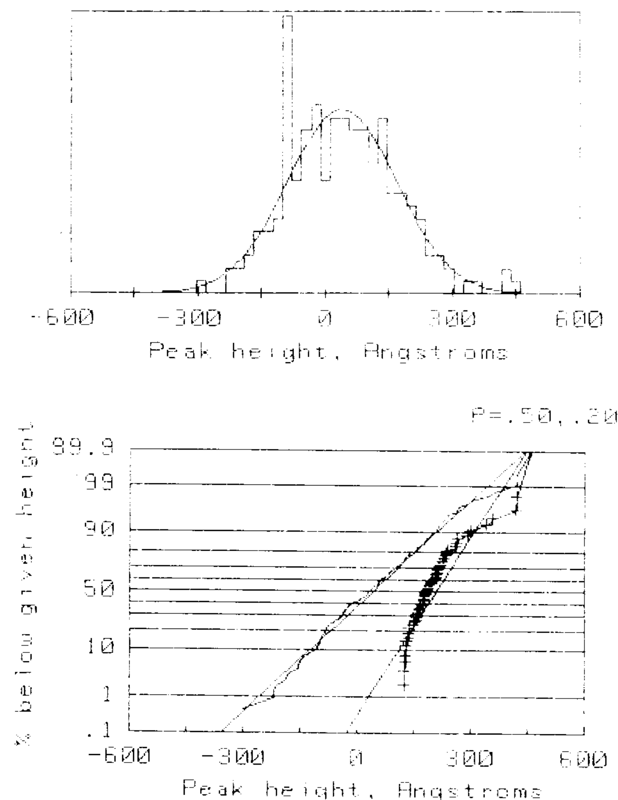

Fig. 3(f)—Histogram and distribution of surface peak heights for Tape A (• all peaks, + upper 25 percent peaks).

the highest height measured. The root-mean-square (rms) of the height distribution is also calculated.

Histogram of Surface Heights

To calculate the histogram of surface heights the data are grouped into 41 bins. We used the rms surface height and the fact that the average surface height is zero to calculate and plot the Gaussian height distribution for the data.

Surface Height Plot on Probability Paper

This shows the surface-height distribution in histogram form, as well as the height distribution plotted on probability paper. The plot shows the percentage of the surface below a given height. Also shown on the plot is a straight line corresponding to a normal distribution of surface heights. The slope of the straight line is determined by the rms surface height, while the position of the line for 50 percent probability is set at the average height value, which for this plot is zero.

The goodness of the fit between the height distribution (and all subsequent distributions also) and the normal distribution is calculated using the Kolmogorov-Smirnov test, (*15*) to (*17*). In the Kolmogorov-Smirnov test, the maximum departure between the percentage of the surface above a given height for the data and the percentage of the surface that would be above a given height if the height distribution were a normal distribution is first calculated. Then a calculation is made to determine if, indeed, the height distribution is normal. The level of significance is printed out as the P value at the upper right corner of the graph. P gives the probability of mistakenly or falsely rejecting the hypothesis that the height distribution is a normal distribution. Common minimum values for P for accepting the hypothesis are 0.01 and 0.05 (*17*).

The chi square (χ^2) test, (*17*) or (*18*), was also evaluated to determine how well the surface height distribution matched a normal distribution. However, the χ^2 test did not prove useful because the goodness of fit calculated depended too much upon how many bins or discrete cells the surface height data were divided into.

Autocovariance Function

The autocovariance function for the surface-height distribution is calculated by first performing a Fast Fourier transform of the surface-height distribution, squaring this result, and then performing an inverse Fast Fourier transform. Two correlation distances are calculated and printed out on the graph. The first correlation distance shown gives the distance for the autocovariance function to drop to 0.1 of its maximum value, while the second correlation distance is the distance for which the autocovariance function first drops to zero.

The correlation coefficient between the autocovariance function and exponential autocovariance function* is calculated. To obtain this correlation coefficient, the natural logarithm of the autocovariance function is calculated and the correlation between this result and a straight line is determined.

Surface Slopes and Curvatures

Histograms and plots on probability paper are made for the surface slope data. The surface slopes are calculated by

*Whitehouse and Archard (*3*) have assumed the autocovariance function of most surfaces to be exponential.

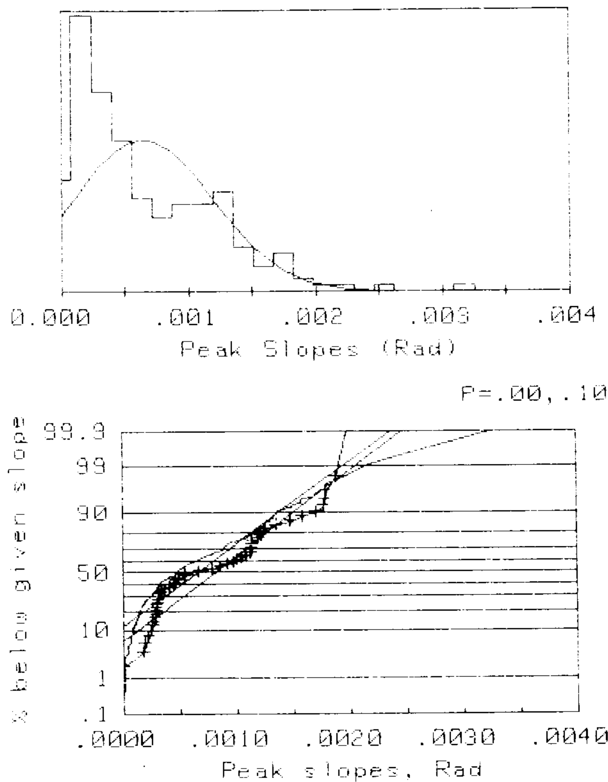

Fig. 3(g)—Histogram and distribution of peak slopes for Tape A (• all peaks, + upper 25 percent peaks).

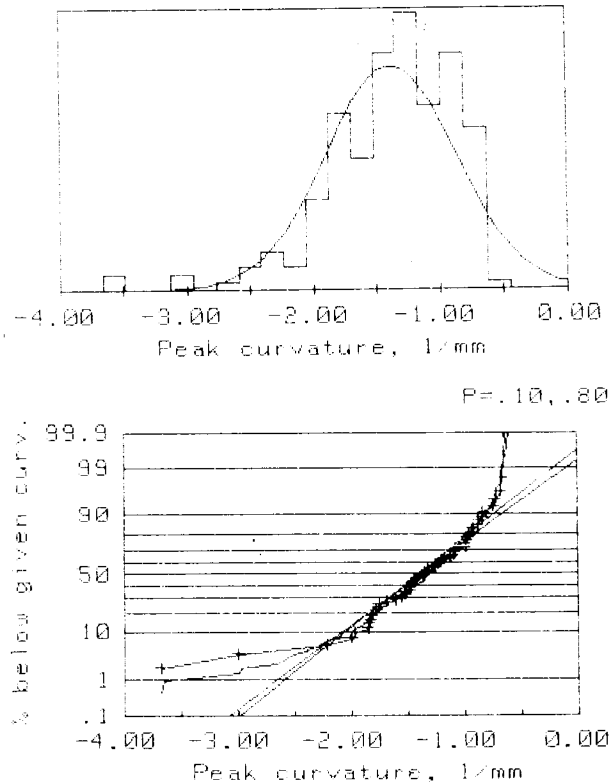

Fig. 3(h)—Histogram and distribution of peak curvature for Tape A (• all peaks, + upper 25 percent peaks).

finding the height differences between adjacent points across the sample.

Similar plots are made for the surface curvature. The curvature is calculated by finding how the surface slope changes between adjacent points across the sample.

Peaks

A peak is defined as a point higher than its two adjacent points (2). For our calculations, an additional requirement for a point to be considered a peak is that the point be at least 20 angstroms above one of the two adjacent points. The additional requirement was introduced to eliminate effects of noise and to ensure that any of the peaks identified are truly substantial peaks.

Once a peak is identified, the height of the peak is stored, and the curvature of the peak is calculated by looking at the slope between the peak and the points on each side of the peak. The absolute slopes between a peak and adjacent valleys* are also calculated.

The mean, maximum, minimum, and standard deviation for peak height, curvature, radius (1/curvature), and the absolute slope are calculated for all peaks and for the 25 percent highest peaks. (It is believed that in most interactions, the upper 25 percent peaks are those most likely to interact.) Also, the correlation coefficient between height and curvatures, heights and radii of curvature, and heights and log radii of curvature for all peaks and the 25 percent highest peaks are calculated. The number of peaks/mm and the number of peaks/mm^2 are calculated for all peaks and for the peaks above the zero mean of the surface-height distribution. Because the data are taken only along one line, the number of peaks/mm^2 is not measured directly. It is calculated by the following equation (*19*):

$$\text{No./mm}^2 = 1.2\ (\text{No./mm})^2 \qquad [5]$$

The number of times per millimeter the surface profile passes through the zero mean is called "number of zero crossings" and is also calculated. Sample data for two tapes, floppy disk, rigid disk, and Ni-Zn ferrite (ground and lapped) are given in Table 2.

Plots were made for the curvature versus peak height, and radii versus peak height to study any correlations. Histograms and plots on probability paper were made for (1) heights of the surface peaks, (2) curvature of the peaks, and (3) slopes of the peaks. Plots on probability paper were made on the radii of the peaks and the log radii of the peaks.

Resolution, Repeatability, and Accuracy

The lateral resolution of the instrument is on the order of 2 microns. The repeatability of the instrument is on the order of 1 to 10 angstrom rms. The repeatability depends upon how rough the surface is and how good the surface reflectivity is. A typical repeatability for the magnetic media analyzed for this study was 5 angstroms rms. This number was determined by obtaining a surface profile and storing these data in the computer, repeating the measurement of the surface profile, and then subtracting these two profiles and finding the rms of the difference.

To determine the accuracy of the instrument, we have

*A valley is defined as point at least 20 angstroms lower than its two adjacent points.

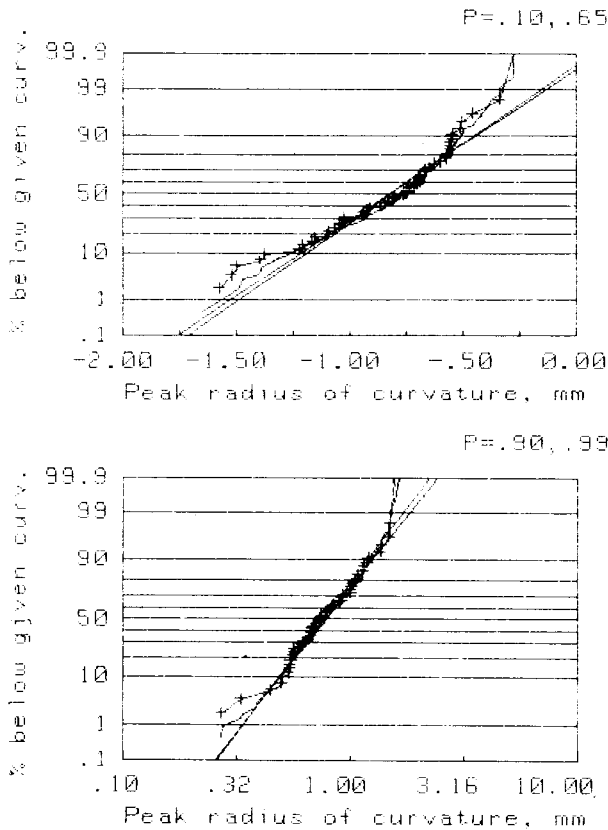

Fig. 3(i)—Distribution of peak radii and peak log radii for Tape A (• all peaks, + upper 25 percent peaks).

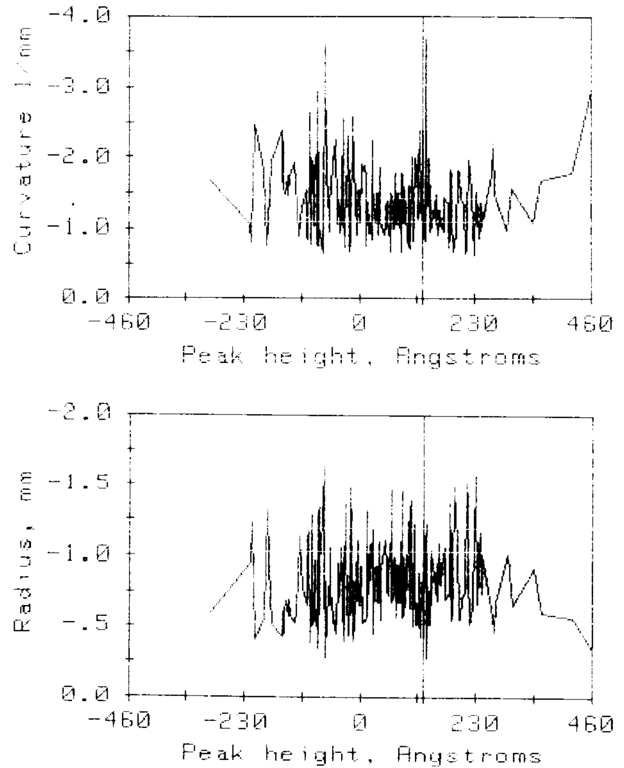

Fig. 3(j)—Curvature and radii vs peak height for Tape A. Upper 25 percent of the peak height values are to the right of the vertical line near 120 angstroms.

compared the measurement of a superior polished surface with measurements performed by Jean Bennett using a modified Talystep instrument at the Naval Weapons Center at China Lake, California (*20*). The two measurements agreed to within 0.7 angstroms rms. The two instruments actually measure somewhat different characteristics, because the optical profilometer has a lateral resolution of two microns and the Talystep has a lateral resolution of 0.1 microns. Our feelings are that, for small height errors, the accuracy of our measurements is within a few (perhaps less than) 10 angstroms.

RESULTS AND DISCUSSION

As mentioned previously, surface area measured in a single trace is 2 microns wide and 0.5 mm long. The first series

TABLE 2—EXPERIMENTAL VALUES OF SURFACE ASPERITY STATISTICS

				PEAKS/UPPER 25% PEAKS										
				HEIGHT		|SLOPE|		CURV.						
SURFACE TYPE	rms SURFACE HEIGHT A^0	rms SURFACE SLOPE $\times 10^{-3}$	rms SURFACE CURVATURE 1/mm	MEAN A^0	ST. DEV. A^0	MEAN $\times 10^{-3}$	ST. DEV. $\times 10^{-3}$	MEAN 1/mm	ST. DEV. 1/mm	PEAK TO VALLEY DISTANCE A^0	P/UP DENSITY /mm²	NUMBER OF P/UP /mm	N_o/mm	ACD 1/ ACD 2 mm
Tape A	136	1.7	0.85	42/ 219	130/ 77	0.6/ 1.0	0.6/ 0.5	1.36/ 1.44	0.52/ 0.55	904	3276/ 1264	52/32	41	0.024/ 0.028
Tape B	261	4.0	1.79	109/ 451	260/ 110	2.0/ 2.5	1.3/ 1.3	2.24/ 2.27	1.03/ 1.00	1218	4407/ 1788	61/39	44	0.026/ 0.030
Rigid Disk	73	1.6	1.16	21/ 113	72/ 43	0.7/ 0.9	0.6/ 0.6	1.43/ 1.53	0.62/ 0.69	491	13180/ 4823	105/63	71	0.012/ 0.015
Floppy Disk	818	13.2	8.21	210/ 1213	816/ 375	8.0/ 9.9	5.2/ 4.7	7.81/ 8.60	5.80/ 5.41	5179	11431/ 4320	98/60	48	0.019/ 0.042
Ferrite	70	2.0	1.50	29/ 107	65/ 36	0.9/ 1.1	0.8/ 0.8	1.71/ 1.93	0.82/ 1.05	462	14626/ 7152	110/77	88	0.032/ 0.034

P/UP—All Peaks/Peaks Above Mean
N_o—No. of Zero Crossings/mm
ACD 1/ACD 2—Autocorrelation distance at which autocovariance function drops to 0.1/drops to 0.0

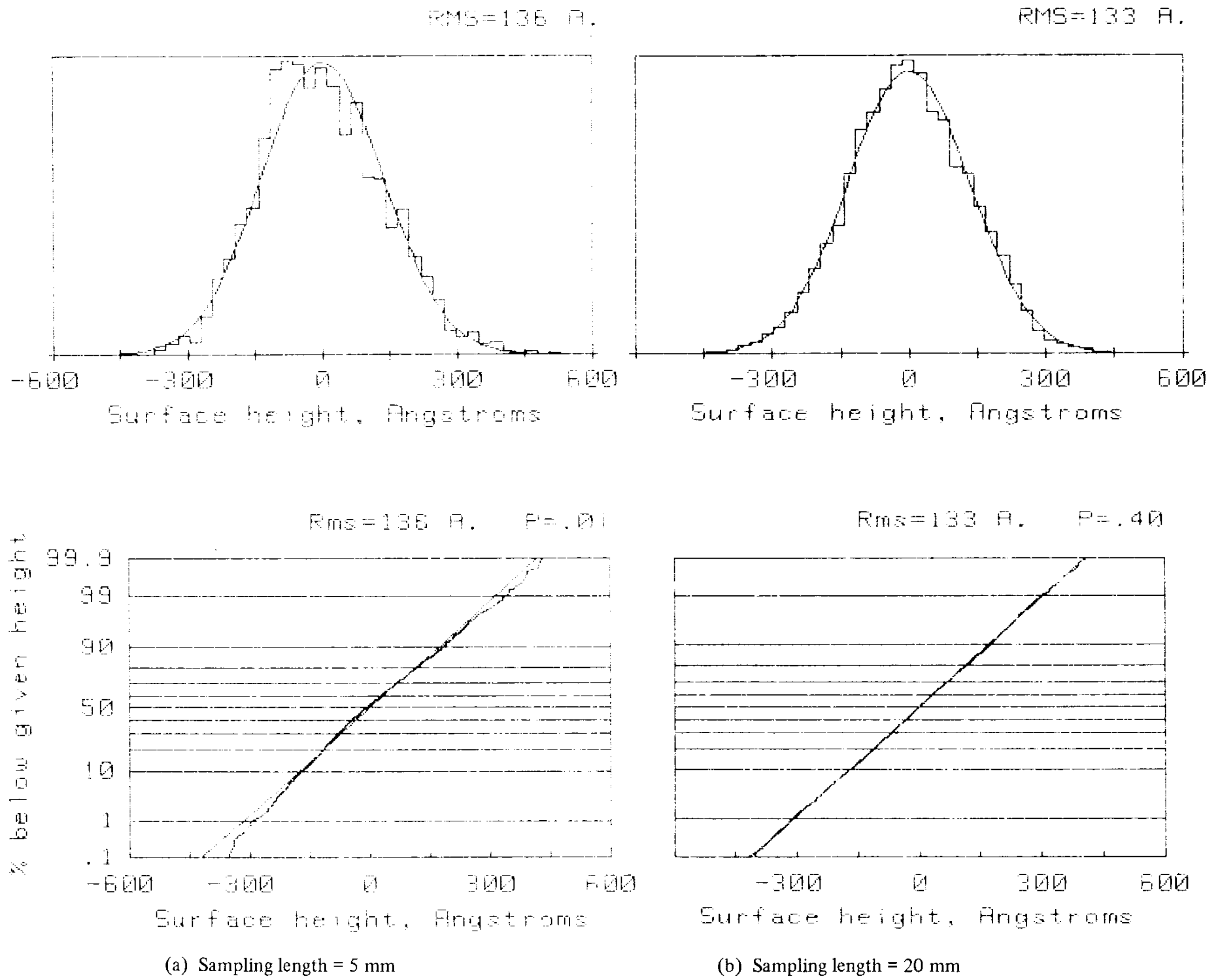

Fig. 4—Histograms and distributions of surface heights for Tape A

of tests were done to determine the statistical sample size. It was also of interest to know if the surface roughness varied from one location to another and if the roughness was isotropic. The test samples selected for this study were two commercially available computer magnetic tapes, A and B (12.7 mm wide and about 30 μm thick). On each tape, 10 runs each were made in the longitudinal direction at three locations about 5 meters apart. In addition, 10 runs were made at the first location in the transverse direction. Surface rms and autocorrelation distance (where the autocorrelation function first becomes zero) were calculated for each run, then net rms and net autocorrelation distances were calculated by adding one run at a time. The data for tape A are plotted in Figs. 4 to 6. From the examination of the histograms in Fig. 4, we note that the surface-height distribution becomes more Gaussian as trace length is increased. From Fig. 5, we note that the rms from one run to another can vary by a factor of 2. However, the net rms for 10 runs at each location is approximately the same. Similar results are obtained for the autocorrelation distance (Fig. 6). Therefore, we concluded that the surface roughness of a tape along its axis and in the transverse direction is comparable and the variation is not statistically significantly from one location to another. Furthermore, about 10 runs should be made to obtain a good statistical sample. The same conclusions were drawn on the second tape.

According to Whitehouse and Archard (*3*), the standard deviation of the mean of an rms data set is given by $\sqrt{1/2M}$

$$\text{where } M = \frac{\text{Sampling Length}}{2.3\beta^*} \qquad [6]$$

$2.3\beta^*$ = autocorrelation distance, where the normalized autocorrelation function $(c(\beta)) = 0.1$

From Eq. [6], we get,

for a 10 percent standard deviation,
sampling length = x50 autocorrelation distance
and for a 5 percent standard deviation,
sampling length = x200 autocorrelation distance

The autocorrelation distance of the tape A is 0.030 mm. Therefore, for rms values with a 5 percent standard deviation, the sampling length should be about 6 mm or 12 data sets. Standard deviation of the 10 data sets plotted in Fig. 5 was 6.2 percent. Therefore, it seems that the theory predicts adequately the sampling length.

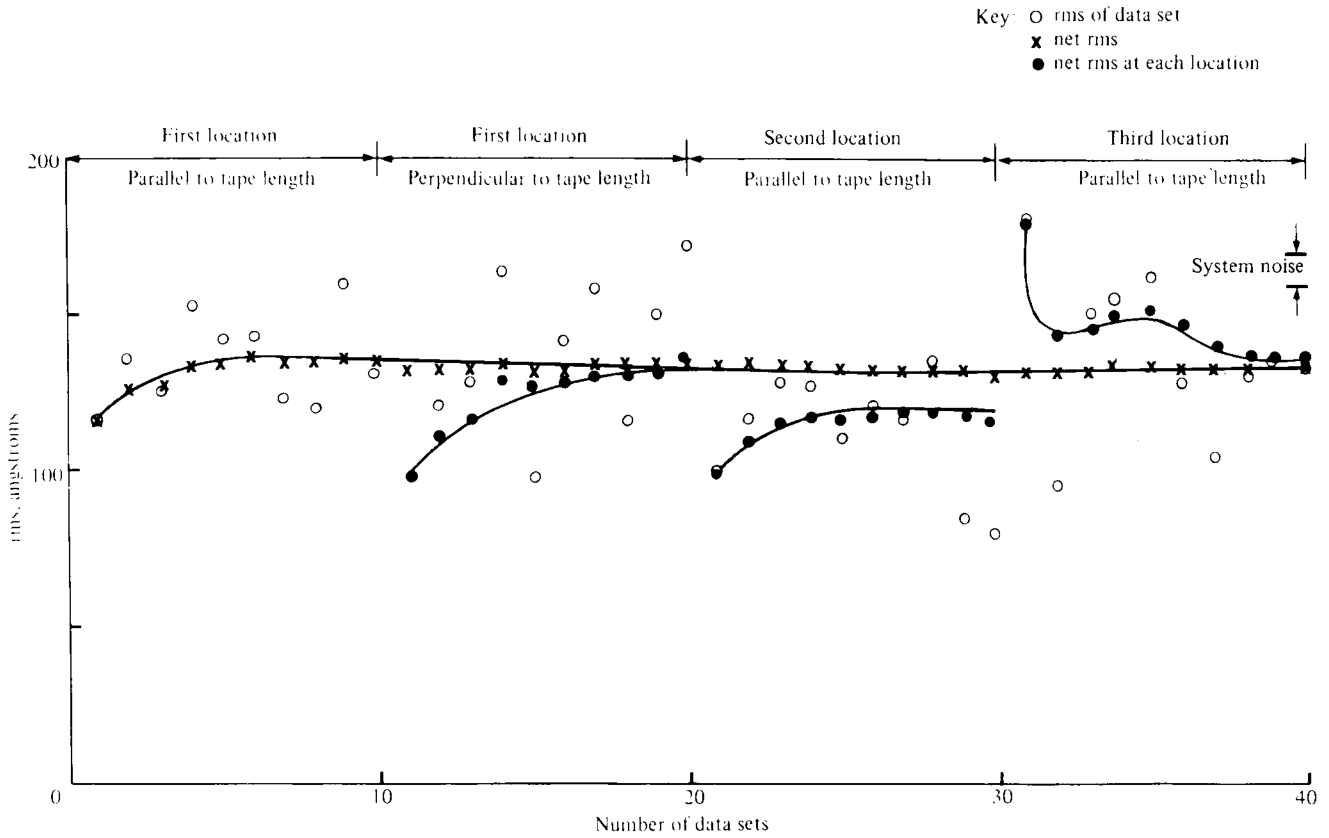

Fig. 5—Variation of rms with number of data sets for Tape A

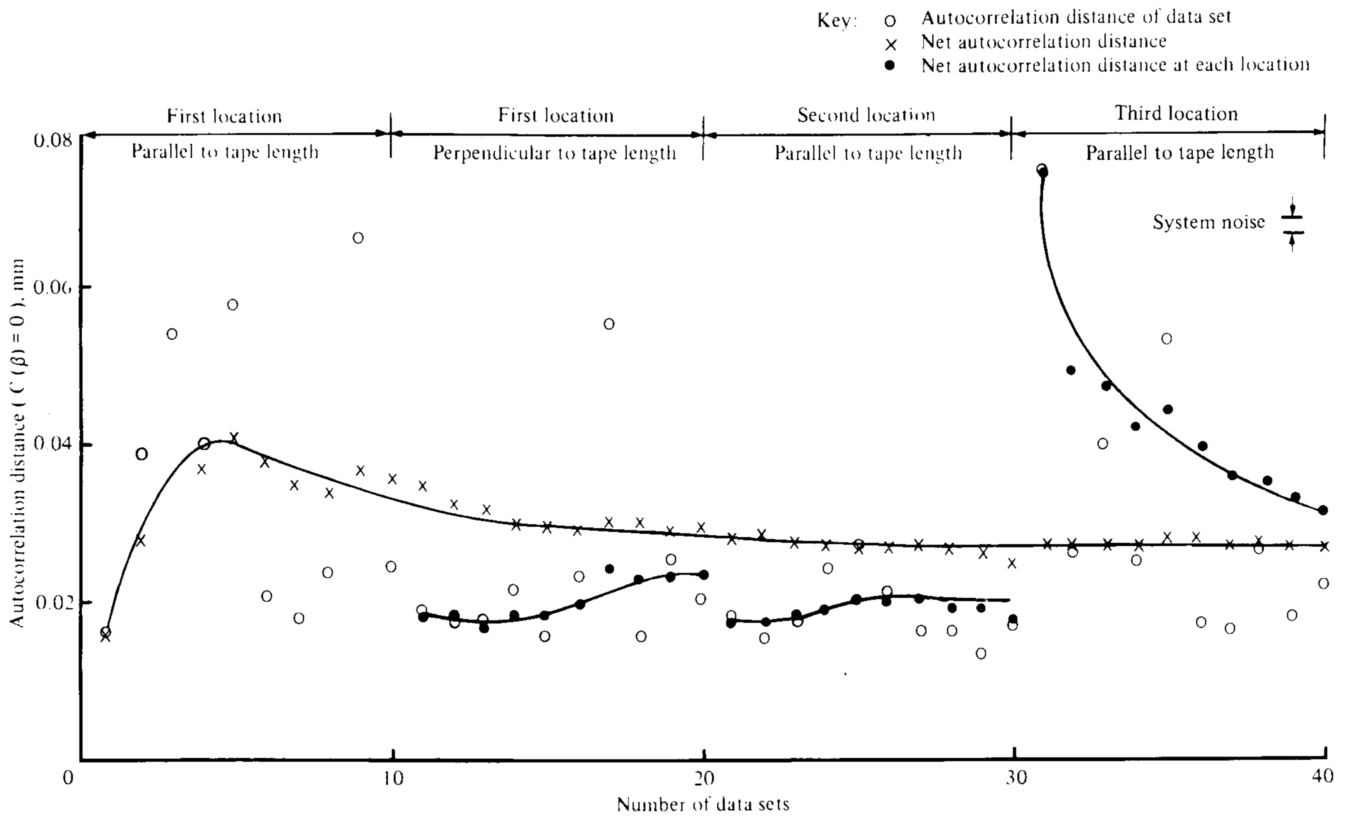

Fig. 6—Variation of autocorrelation distance with number of data sets for Tape A

The sample results of 10 data sets for tape A-heights, slopes and curvatures for all surface and surface peaks are shown in Fig. 3. From examination of plots in Fig. 3 and data of about 20 other computer tapes, we note that surface

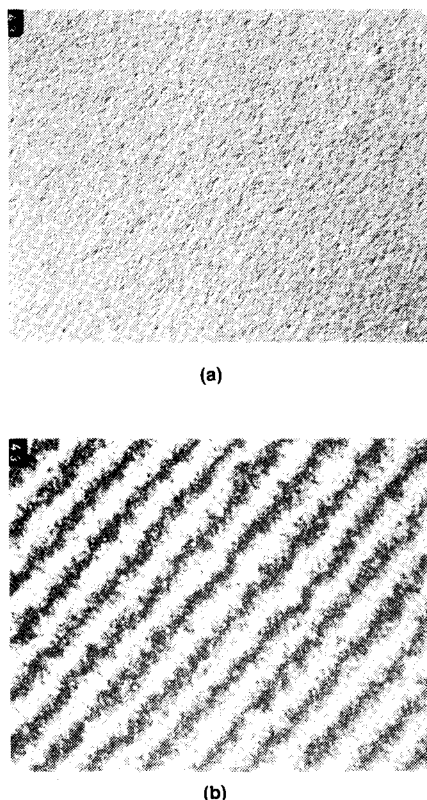

(a)

(b)

Fig. 7(a)—Nomarski DIC photograph for Tape A
(b)—Nomarski polarization interferometer photograph for Tape A

heights, slopes, and curvatures are Gaussian. All the peak heights are Gaussian, and the upper 25 percent peaks are *nearly* Gaussian. However, all peak slopes, curvatures, and radii are *not* Gaussian, and the upper 25 percent peak slopes, curvatures, and radii are *nearly* Gaussian. If we plot all peak and upper 25 percent peak log radii, we note that these are Gaussian [Fig. 3(i)]. Gupta and Cook (*21*) also found that in cases of metals, peak radii have log normal distribution. Figure 3(j) shows that peak height and curvature or radii are not correlated ($|\text{correlation coeff.}| < 0.10$). However, the upper 25 percent peak height and curvature or radii have slightly better correlation ($|\text{correlation coeff.}| \sim 0.2$ to 0.3). Nayak (*19*) has suggested positive correlation exists between curvature and heights. The autocovariance function is found to be exponential. The correlation coefficient between the natural log of the autocovariance and a straight line is generally between 0.95 and 0.99.

The Nomarski differential-interference contrast and the Nomarski polarization interferometer photographs for Tape A are shown in Fig. 7 for comparison. The DIC data are highly qualitative, Tape A appears smooth. Polarization interferometer data are semiquantitative. Mercury green light was used to make the measurement. The spacing between the centers of two adjacent black lines is $\lambda/2 = 0.2731$ µm. Any fluctuations in the lines represent surface irregularities. In Fig. 7(b), on the average, the variations are 1/10 to 3/10 of $\lambda/2$ ($= 0.027$ to 0.082 µm). A rule of thumb for calculating CLA (center-line average) is to divide this number by 4, therefore, CLA is about 0.014 µm. Here, the average topography information is available over a large area. (The photograph in Fig. 7(b) was taken at a magnification of 170, which allows variations over a minimum length of about 25 µm to be resolved).

Correlation Between Gloss Number and Net rms of Surface Heights

Because the gloss number is commonly used to characterize magnetic tapes, it is of interest to find a correlation between the gloss number and the net rms of surface heights obtained with the optical profilometer.

The glossmeter measures the specular reflectance (or gloss) of the surface (roughly 50 mm × 50 mm), which is simply the fraction of the incident light reflected from a surface when the angles of incidence and reflectance are equal numerically but opposite in sign (*7*). The ideal black glass (refractive index = 1.567; Fresnel reflectance for unpolarized radiation for 60° = 0.100) is assigned an arbitrary number of 100 at all incident angles. Specular reflectance increases with an increase in the refractive index (see the Appendix) and patches of the surface not in the reflecting plane scatter the reflected light, some of which misses the detector completely, (*22*) to (*25*). Therefore, gloss depends on both the refractive index of the surface and the surface texture for a given angle of view.

A number of tapes (12.7 mm in width) were selected for this study. Gloss measurements were made at an angle of incidence of 45° and the aperture was 9.5 mm × 50 mm. Six gloss readings were taken at different locations on each tape sample and the variation generally was within one point. A plot of gloss numbers versus rms is given in Fig. 8. We note that there is a poor correlation between the gloss number and the rms for different tape formulations and a barely acceptable one for a single tape formulation. In the case of different tape formulations, this is caused by variation of reflectivity (refractive index) from one tape formulation to another. In the case of a single tape formulation, there might be changes in the reflectivity from tape to tape caused by the variation of magnetic-particle distribution or level of polishing of the binder system. The refractive indexes of a typical polymer-binder system and magnetic particles are 1.45 to 1.6 and 1.6 to 1.85, respectively.

The refractive index of the polymer depends on the dipole moment, which does not vary with the temperature (unless near half the melting point), but it can vary with humidity caused by the deposition or adsorption of water molecules. Therefore, the gloss number could depend on the environmental exposure to the sample. [Aging of pigments leading to different gloss numbers have been reported in (*25*)]. To study the influence of the environment on gloss number, two tapes were subjected to different humidity and temperature conditions. The results are reported in Table 3. We note that if the tape is exposed to either high temperature or high humidity for several weeks, the gloss number decreases. The net rms values did not change because of the exposure. The refractive index of tapes were measured using Gaertner Scientific ellipsometer (Model HP 9845B, 4mW HeNe Laser, substrate program No. GP5A). The tapes having lower gloss numbers had lower refractive indexes. Therefore, we believe that change

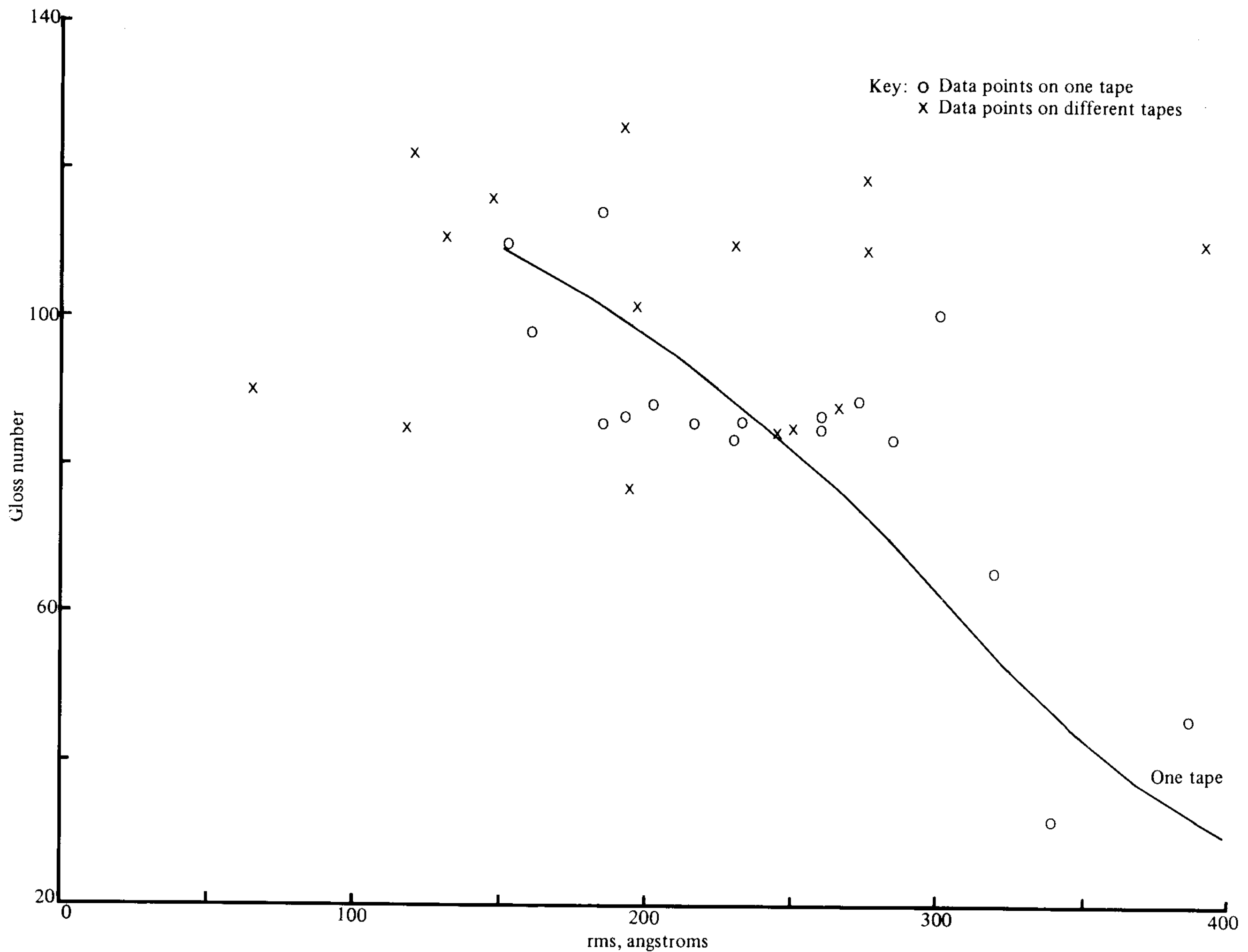

Fig. 8—Gloss number vs rms comparison for several tapes

TABLE 3—EFFECT OF ENVIRONMENTAL EXPOSURE TO GLOSS NO. AND REFRACTIVE INDEX OF MAGNETIC TAPES

Tape Designation	Temp. °C / Relative Humidity %	No. of Days	Gloss Number	Refractive Index		
				Real	Imag.	Total
Tape B	Ambient		85	1.82	0.39	1.86
	60/85	1	85	1.74	0.63	1.85
Tape C	Ambient		114	1.88	0.59	1.97
	52/60	7	112	1.87	0.62	2.03
	52/60	21	104	1.65	0.65	1.77
	52/60	45	104	1.70	0.56	1.79
	52/30	7	113	1.88	0.60	2.04
	52/30	21	110	1.87	0.60	1.97
	52/30	45	101	1.63	0.69	1.83
	23/60	7	108	1.88	0.60	1.98
	23/60	21	108	1.88	0.60	1.97
	23/60	45	100	1.65	0.71	1.79

There was no change in net rms because of environmental exposure.

in the gloss number is the result of changes in the refractive index of the tapes rather than changes in surface topography.

Peak-to-Valley Versus Net rms for Magnetic Tapes

In magnetic-recording technology, it is of great interest to know the peak-to-valley distance because the flying height is on the same order. Peak-to-valley distance and net rms data on more than 100 commercially available tape samples (new and worn) were plotted in Fig. 9. At least square fit resulted in the following relation:

$$\text{Peak-to-valley distance (A°)} = 6.06\ (\text{net rms, A°}) - 76;\ \text{A°}$$

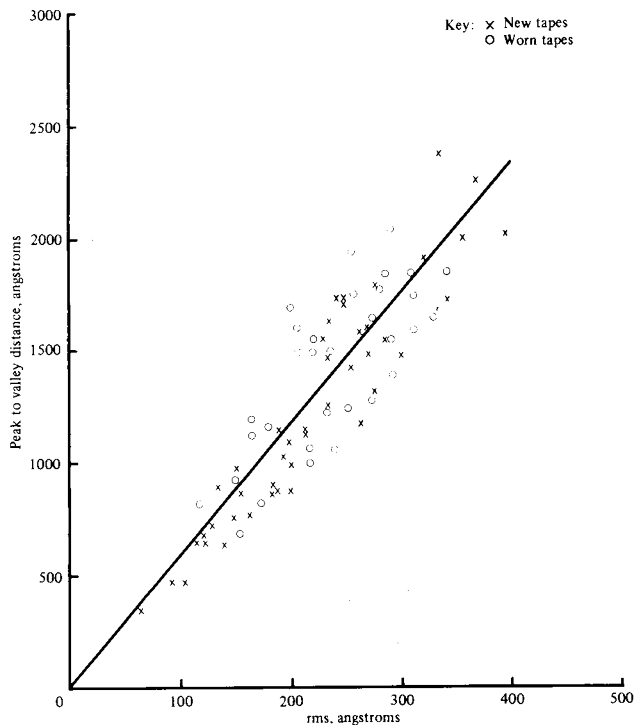

Fig. 9—Correlation between peak-to-valley distance versus net rms

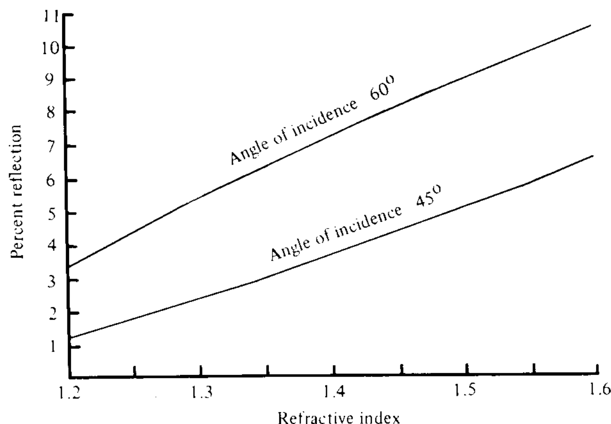

Fig. 10—Relation between percent reflection and refractive index of dielectric materials.

Therefore, the peak-to-valley distance is approximately 6 times the net rms, or, the height of the highest peak from the mean is about 3 times the net rms. This is what one would expect for a Gaussian distribution where 99 percent of the surface heights lie within ± three times the rms (σ).

CONCLUSIONS

A noncontact, surface-profile-measurement technique has been successfully developed using Mirau interferometry. From the measured surface-height distribution, surface-topography data are calculated, which can be used for predictions of tribological and magnetic performances of magnetic media. A tape surface of about 5 mm in length (×200 autocorrelation distance) needs to be examined for a good statistically sample.

For magnetic tapes, surface heights, slopes, and curvatures have Gaussian distributions. Peak heights are nearly Gaussian, but peak slopes, curvatures, and radii are not Gaussian. Peak radii follow a log normal distribution. Peak heights and radii did not correlate. The autocovariance function was found to be exponential. The peak-to-valley distance on a magnetic-tape surface is found to be roughly six times the net rms.

Correlation of net rms with a commonly used glossmeter technique is poor, and Nomarski techniques as used today give only semiquantitative information. Therefore, the optical profilometer described in this paper is more suitable for more accurate and detailed measurements of soft substrates.

REFERENCES

(1) Bowden, F. P. and Tabor, D., *Friction and Lubrication of Solids*, Oxford University Press (1954).

(2) Greenwood, J. A. and Williamson, J. B. P., "Contact of Nominally Flat Surfaces," *Proc. R. Soc. Lond.*, Series A, **295**, pp 300–319 (1966).

(3) Whitehouse, D. J. and Archard, J. F., "The Properties of Random Surfaces of Significance in Their Contact," *Proc. R. Soc. Lond.*, Series A, **316**, pp 97–121 (1970).

(4) Whitehouse, D. J. and Phillips, M. J., "Discrete Properties of Random Surfaces," *Proc. R. Soc. Lond.*, Series A, **290**, pp 267–98 (1978).

(5) Special issue on Metrology and Properties of Engineering Surfaces, *Wear*, **57**, pp 1–384 (1979).

(6) Williamson, J. B. P., "Topography of Solid Surfaces," *Proc. of NASA Symposium on Interdisciplinary Approach to Friction and Wear*, NASA SP-181, pp 85–142.

(7) Gardner, H. A. and Sward, G. G., *Paint Testing Manual, Physical and Chemical Examination: Paints, Varnishes, Lacquers and Colors*, Gardner Lab. Inc., Bethesda, Maryland.

(8) Francon, F., *Optical Interferometry*, Academic Press, NY (1966).

(9) Francon, F. and Mallick, S., *Polarization Interferometers*, Wiley Interscience, NY (1971).

(10) Tolansky, S., *Introduction to Interferometry*, Wiley, NY, pp 213–214 (1973).

(11) Bruning, J. H., "Fringe Scanning Interferometers," *Optical Shop Testing*, Ed. by D. Malacara, Wiley, NY, pp 409–437 (1978).

(12) Sommargren, G. E., "Optical Heterodyne Profilometry," *Appl Opt.*, **20**, pp 610–618 (1981).

(13) Wyant, J. C. and Koliopoulos, C. L., "Phase Measurement System for Adaptive Optics," *Agard Conf. Proc.* No. 300, 48.1–48.12 (1981).

(14) Wyant, J. C., "Use of and AC Heterodyne Lateral Shear Interferometer With Real Time Wavefront Corrections System," *Appl. Opt.*, **14**, 11, pp 2622–2626 (1975).

(15) Smirnov, N., "Table for Estimating the Goodness of Fit of Empirical Distributions," *Annals of Mathematical Statistics*, **19**, pp 279–281 (1948).

(16) Massey, F. J., "The Kolmogorov-Smirnov Test for Goodness of Fit," *J. Amer. Statist. Assoc.*, **46**, pp 68–79 (1951).

(17) Siegel, S., *Nonparametric Statistics for the Behavioral Sciences*, McGraw Hill (1956).

(18) Breiman, L., *Statistics: With a View Toward Applications*, Houghton-Mifflin, Boston, pp 187–206 (1973).

(19) Nayak, P. R., "Random Process Model of Rough Surfaces," *J. Lub. Tech., Trans. ASME*, **93F**, pp 398–407 (1971).

(20) Bennett, J. M. and Dancy, J. H., "Stylus Profiling Instrument for Measuring Statistical Properties of Smooth Optical Surfaces," *Appl. Opt.*, **15**, pp 1785–1802 (1981).

(21) Gupta, P. K. and Cook, N. H., "Statistical Analysis of Mechanical Interaction of Rough Surfaces," *J. Lub. Tech., Trans. ASME*, **94F**, pp 19–26 (1972).

(22) Budde, W., "Polarization Effects in Gloss Measurements," *Applied Optics*, **18**, 13, July, pp 2252–2256 (1979).

(23) Bennett, H. E. and Porteus, J. O., "Relation Between Surface Roughness and Specular Reflectance at Normal Incidence," *J. Opt. Soc. Amer.*, **51**, pp 123–129 (1961).

(24) Hecht, E. and Zajac, E., *Optics*, Addison Wesley, p 82 (1974).

(25) Alince, B. and Lepoutre, P., "Plastic Pigments in Paper Coatings," *Tappi*, **63**, 5, May, pp 49–53 (1980).

APPENDIX

Fresnel's equations, which are usually given for the refractive index, angle of incidence, and angle of refraction, were rewritten by means of Snell's law to give the total reflectance (R) of a *dielectric* surface for *unpolarized* incident radiation as follows (*24*),

$$R = (R_1 + R_2)/2 \quad [7]$$

with

$$R_1 = \left[\frac{\mathrm{Cos}\ \alpha - (n^2 - \sin^2\alpha)^{1/2}}{\mathrm{Cos}\ \alpha + (n^2 - \sin^2\alpha)^{1/2}}\right]^2 \quad [8]$$

and

$$R_2 = \left[\frac{n^2\cos\alpha - (n^2 - \sin^2\alpha)^{1/2}}{n^2\cos\alpha + (n^2 - \sin^2\alpha)^{1/2}}\right]^2 \quad [9]$$

where n is the refractive index of the dieletric material, α is the angle of incidence, and R_1 and R_2 are the reflectance in the perpendicular and the parallel to the incident plane, respectively. It should be noted that the above equations are strictly valid for dielectric surfaces only. Magnetic particles complicate the situation.

For $\alpha = 0$, Eq. [7] reduces to

$$R = \left(\frac{1-n}{1+n}\right)^2 \quad [10]$$

Equation [7] is plotted in Fig. 10 for two commonly used angle of incidences of 45° and 60° in gloss measurements.